Electronic Supplementary Material (ESI) for Soft Matter.

Supporting Information

Rheological implications of pH induced particle-particle association in aqueous suspension of an anisotropic charged clay

Mohammad Shoaib, Erin R. Bobicki*

Department of Chemical Engineering and Applied Chemistry, University of Toronto, Toronto, Ontario, Canada M5S 3E5

*Corresponding author, email: erin.bobicki@utoronto.ca

Kaolinite characterization

Atomic force microscopy was carried out to determine the size and thickness of kaolinite particles. The surfaces of freshly cleaved, high-grade (V-1), 12 mm mica discs (Ted Pella Inc., Redding, CA) were treated for 5 min with 10 µL 3-aminopropyl-trietoxy silane (1 µM in deionized [DI] water), rinsed with 2 mL DI water, and blow dried. A 10 µL drop of 0.025 mg/mL kaolinite suspension was incubated for 5 min on the mica discs inside a wet chamber to avoid desiccation. Discs were dried in a laboratory hood at room temperature and scanned immediately after preparation on a BioScope™ II atomic force microscope (Bruker Corporation, Billerica, MA). High-resolution images of kaolinite particles were obtained using RTESP cantilevers (f_o=237–289 kHz, k=20–80 N/m, Bruker Corporation, Billerica, MA). The particle nanotopography was determined using the tapping mode in air at a 0.7 Hz scan rate. Particle analysis, size distribution, and three-dimensional images were obtained with NanoScope Analysis© software (Ver. 1.50, Bruker Corporation, Billerica, MA).

Scanning electron micrographs were obtained by drying a very dilute suspension of kaolinite on a glass slide then imaging with a Hitachi SU 8230 field emission gun scanning electron microscope. Samples were imaged "as is" with no additional conductive coating.

X-ray diffraction was used to determine the minerology of the kaolinite sample (MiniFlex 600, Rigaku, Japan) using Cu-Kα radiation (λ = 1.5406 Å) and the data was obtained at scan speed of 1.5°/min, at a diffraction angle (2θ) ranging from 5°to 100° and a step size of 0.02°. The pattern is similar to low-defect source kaolinites KGa-1a and KGa-1b[1] (Figure S1).

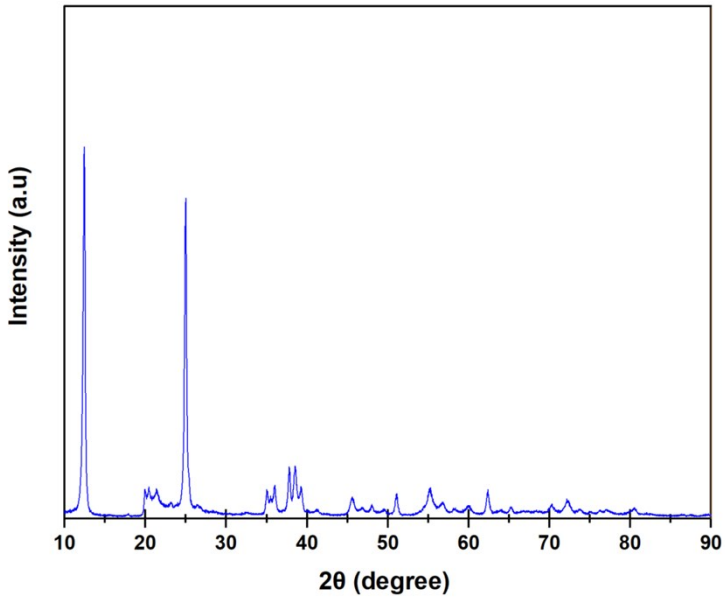

Figure S1 X-ray diffraction pattern of kaolinite sample.

DLVO

Hamaker Constant

Hamaker constants for different interactions is provided in Table S1.

Table S1: Hamaker constants for interactions between surfaces of kaolinite through water from Gupta et al. [2]

Interaction type	*Hamaker constant ($J \times 10^{-20}$)*
Silica face–silica face	1.11
Edge–edge	2.37
Alumina face–alumina face	3.90
Silica face–edge	1.63
Alumina face–silica face	2.08
Alumina face–edge	3.05

Surface potentials

The surface potentials (Table S2) depend on several factors (e.g., type of kaolinite, salinity). However, the IEP of alumina (~pH 6 [3–4]) controls the most attractive interaction (alumina face–silica face). Liu et al. [5] determined that the isoelectric point (IEP) of the kaolinite edge was pH <

4. Since the IEP of pure silica is close to pH 2 and the edge contains both the silica and alumina, we took the IEP of the edge was pH 3[6]. Since ionic strength lowers the potential, the potential of the alumina face was also reduced at pH 2 and 3.1 from the level at pH 4.7.

Table S2: Surface potentials of alumina and silica face and edge of kaolinite at different pH values.

pH	Surface potential (mV)		
	Alumina face[3, 7]	Edge[5]	Silica face[3]
2.0	20	7	0.1
3.1	36	–2.3	–30
4.7	40	–42	–45
5.0	22	–45.7	–49
5.2	20	–47.7	–49.5
5.4	18	–49.4	–51
5.6	15	–50.7	–53
6.0	3	–52.6	–55
8.0	–11.6	–55.8	–63
10	–30.7	–60.5	–65

Two-step yielding

Table S3: Elastic stress and corresponding strain values associated with two-step yielding for kaolinite suspensions in acidic pH regime.

	1st Yielding		2nd Yielding	
pH	**Strain%**	**G'*strain (Pa)**	**Strain%**	**G'*strain (Pa)**
2	0.447	14.58	206.97	12.71
3.1	0.179	9.39	203.71	12.97
4.7	0.115	12.67	264.101	10.45
5	0.073	12.67	200.55	11.04
5.2	0.283	11.71	197.74	7.79

DLVO interaction energy under the Constant charge boundary condition

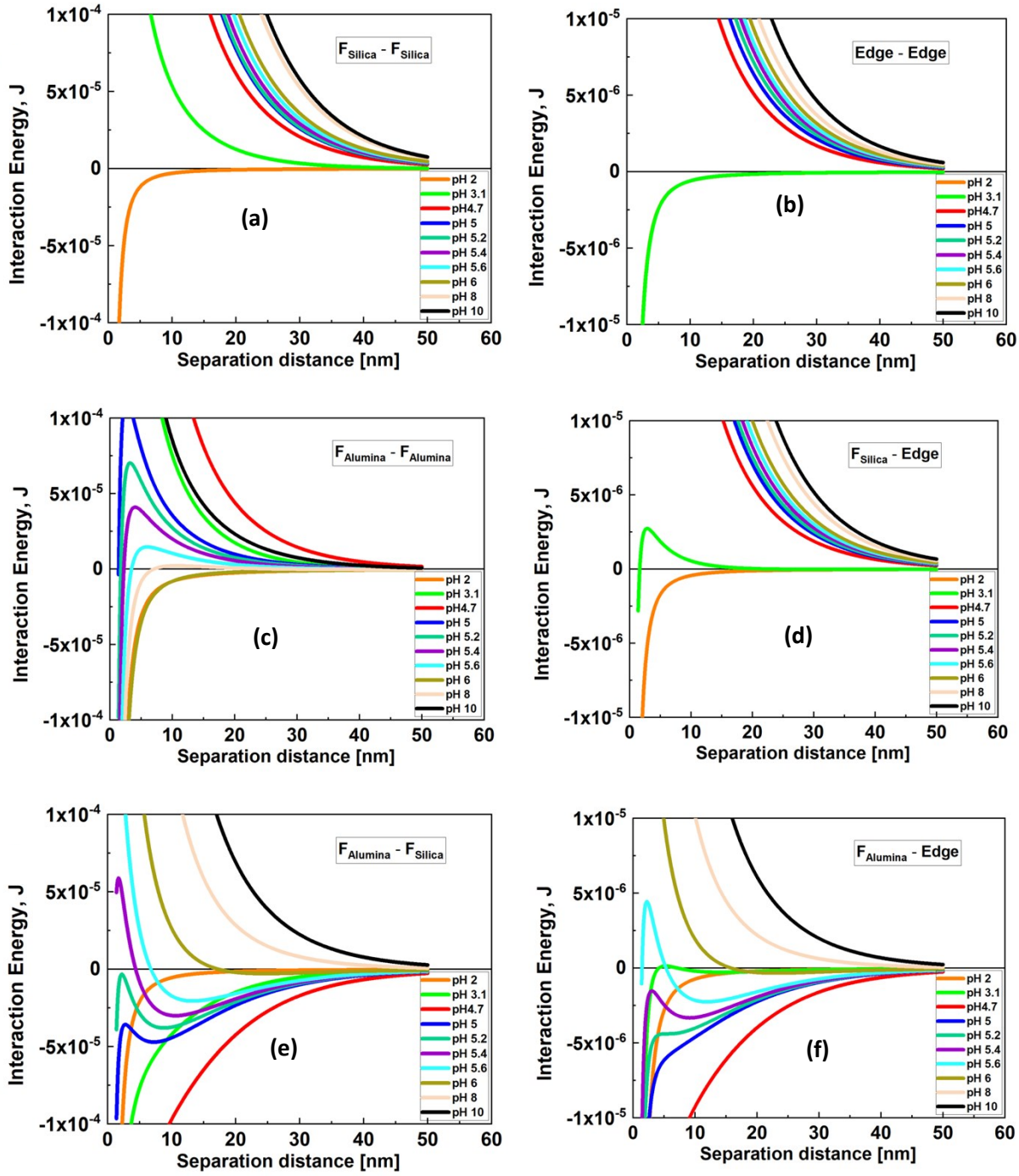

Figure S2 Interaction energy per unit area between kaolinite surfaces at various pH values estimated under the constant charge boundary condition: (a) silica–silica face (b) edge–edge (c) alumina–alumina face (d) silica face–edge (e) alumina face–silica face, and (f) alumina face–edge.

Scaled DLVO interaction.

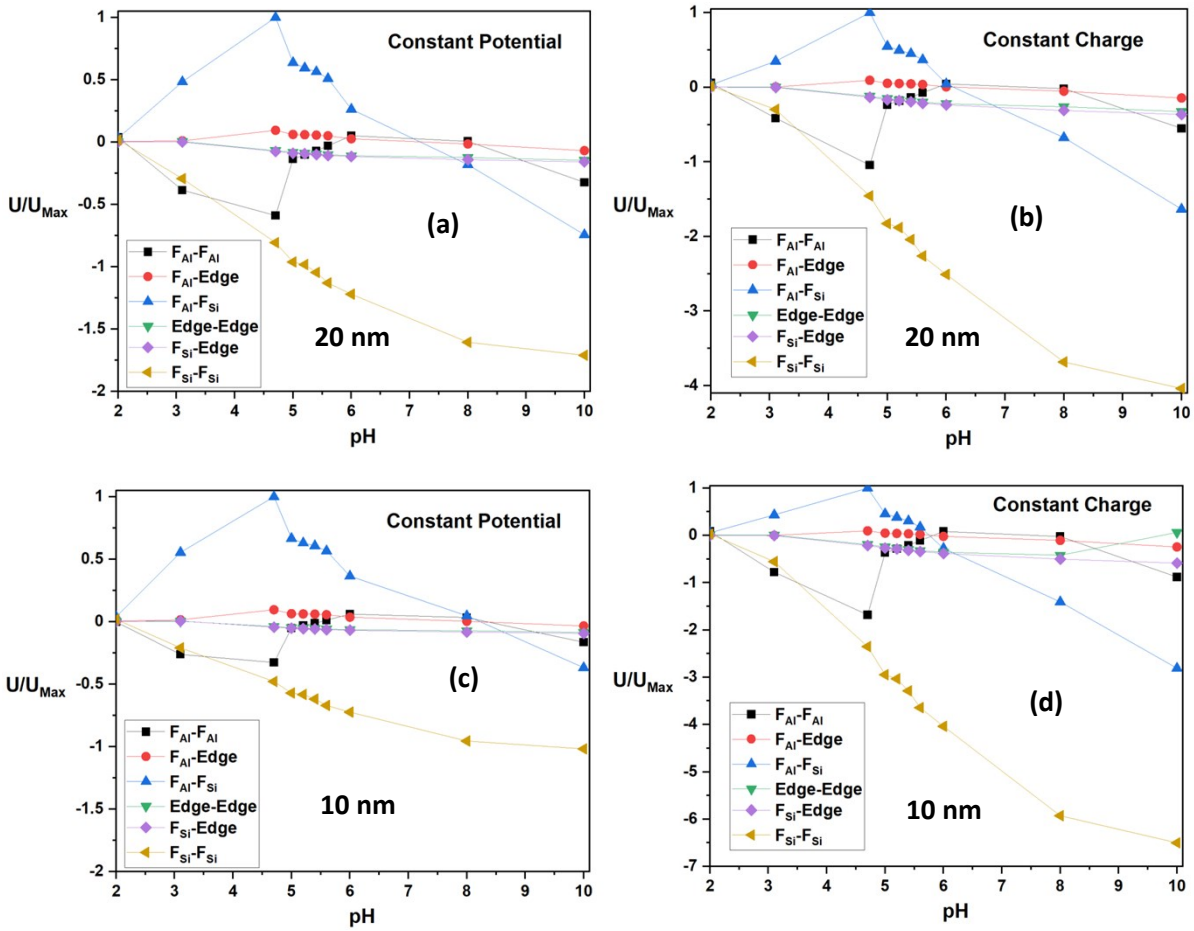

Figure S3 DLVO interaction energy of different interactions scaled to the maximum attractive energy for the alumina face–silica face interaction at (a) 20 nm and (c) 10 nm separation based on the constant potential boundary condition of EDL interaction and at (b) 20 nm and (d) 10 nm separation based on the constant charge boundary condition of EDL interaction.

Rheology experimental limits

Instrument inertia

The minimum viscoelastic moduli required to overcome the instrument inertia were calculated from equation S1 by Ahuja and Gamonpilas[8]

$$G > IK_{\sigma}\omega^2/K_{\gamma} \tag{S1}$$

where, K_{σ} (16243.3 Pa/N.m) and K_{γ} (12.18) are the stress and strain constants respectively, and ω is the frequency.

Low-torque limit

The low-torque limit (T_{min}) of the rheometer sets the minimum measurable viscoelastic modulus, which for the Discovery HR-2 rheometer (TA Instruments, New Castle, DE) is 2 nN.m for oscillatory flow. From this, the limit of viscoelastic modulus as a function of strain amplitude is given by equation S2: [8]

$$G_{min} = K_{\sigma}T_{min}/\gamma \tag{S2}$$

where, K_{σ} (16243.3 Pa/N.m) is the stress constant and γ is the strain amplitude.

Sample inertia

During the frequency sweep, the minimum viscoelastic modulus required to overcome the sample inertia limits is given by equation S3: [9]

$$|G^*| > \left(\frac{10}{2\pi}\right)^2 cos^2(\delta/2)\rho\omega^2 D^2 \tag{S3}$$

where, ρ is the effective sample density (1660 kg/m²), ω is the frequency (Hz), and D is the geometry gap (1.2 mm). The front factor weakly depends on δ and its limit is $1/2 < cos^2(\delta/2) < 1$. We took this factor to be 1 for our calculations, similar to Ewoldt et al.[9].

Difference between Na_2CO_3 and $Ca(OH)_2$ as pH modifier

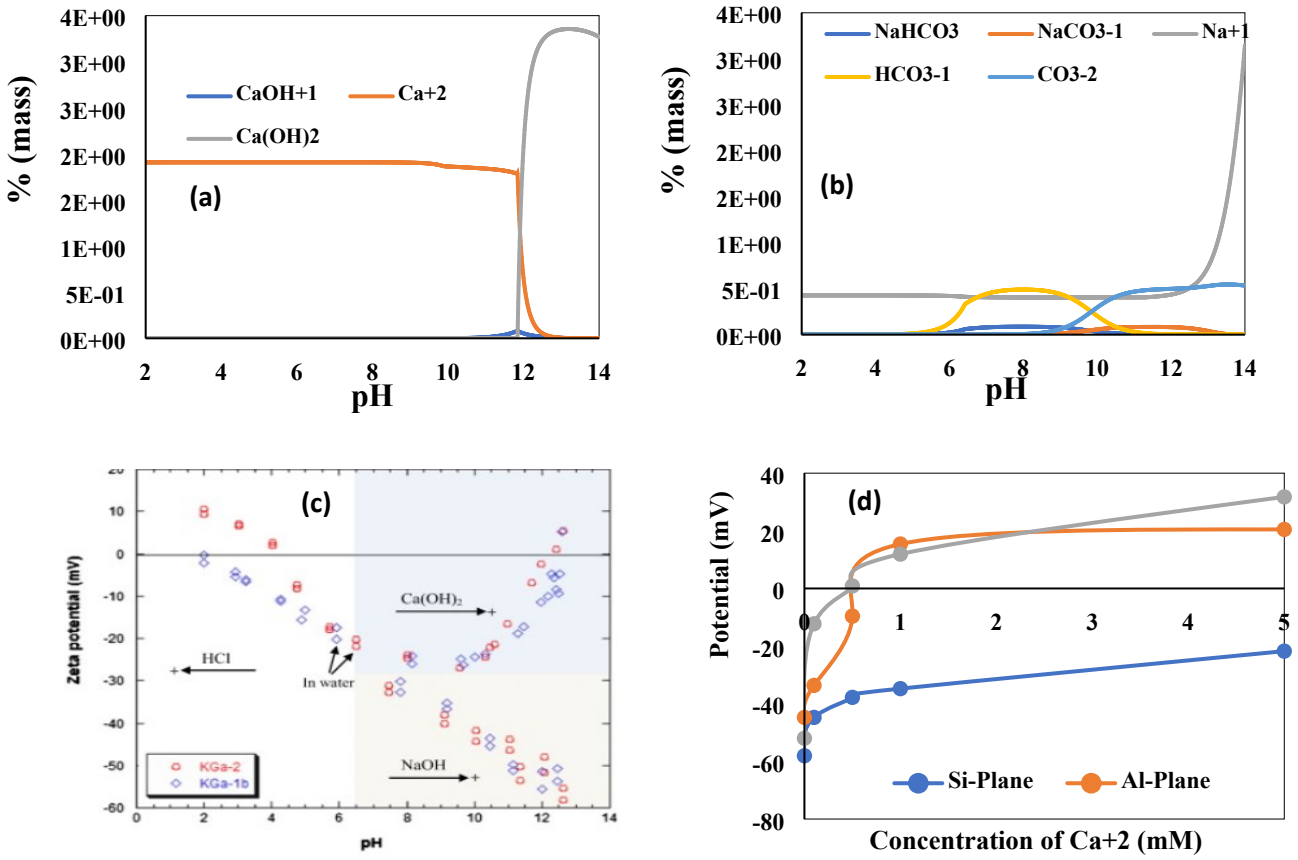

Figure S4 (a) Concentration diagram for $Ca(OH)_2$—Water System and (b) Na_2CO_3—Water System (c) Zeta potential of kaolinite as a function of pH in the presence of $Ca(OH)_2$ and NaOH(Used with permission from Elsevier[10]) (d) Stern potential of Al-face, Si-face and edge as a function of Ca^{+2} concentration[11]

References

1. B. A. Sakharov, V. A. Drits, D. K. McCarty and G. M. Walker, *Clays and Clay Minerals*, 2016, **64**, 314-333.
2. V. Gupta, M. A. Hampton, J. R. Stokes, A. V. Nguyen and J. D. Miller, *Journal of Colloid and Interface Science*, 2011, **359**, 95-103.
3. J. Chang, H. Shao, B. Liu, R. Manica, Z. Li, Q. Liu and Z. Xu, *Journal of Colloid and Interface Science*, 2021, **582**, 439-445.
4. V. Gupta and J. D. Miller, *Journal of Colloid and Interface Science*, 2010, **344**, 362-371.
5. J. Liu, L. Sandaklie-Nikolova, X. Wang and J. D. Miller, *Journal of Colloid and Interface Science*, 2014, **420**, 35-40.
6. G. V. Franks, *Journal of Colloid and Interface Science*, 2002, **249**, 44-51.
7. N. Kumar, M. P. Andersson, D. van den Ende, F. Mugele and I. Siretanu, *Langmuir*, 2017, **33**, 14226-14237.
8. A. Ahuja and C. Gamonpilas, *Colloid and Polymer Science*, 2021, **299**, 165-176.
9. R. H. Ewoldt, M. T. Johnston and L. M. Caretta, in *Complex Fluids in Biological Systems: Experiment, Theory, and Computation*, ed. S. E. Spagnolie, Springer New York, New York, NY, 2015, DOI: 10.1007/978-1-4939-2065-5_6, pp. 207-241.
10. Y. C. Chemeda, D. Deneele, G. E. Christidis and G. Ouvrard, *Applied Clay Science*, 2015, **107**, 1-13.
11. J. Chang, Doctor of Philosophy, University of Alberta, 2019.